

Enhanced Direct CP Violation in $B^\pm \rightarrow \rho^0 \pi^\pm$

X.-H. Guo^{1*}, O. Leitner^{1,2†}, A.W. Thomas^{1‡}

¹ Department of Physics and Mathematical Physics, and

Special Research Center for the Subatomic Structure of Matter,

Adelaide University, Adelaide 5005, Australia

² Laboratoire de Physique Corpusculaire, Université Blaise Pascal,

CNRS/IN2P3, 24 avenue des Landais, 63177 Aubière Cedex, France

Abstract

We study direct CP violation in the hadronic decay $B^\pm \rightarrow \rho^0 \pi^\pm$, including the effect of $\rho - \omega$ mixing. We find that the CP violating asymmetry is strongly dependent on the CKM matrix elements, especially the Wolfenstein parameter η . For fixed N_c (the effective parameter associated with factorization), the CP violating asymmetry, a , has a maximum of order 30% – 50% when the invariant mass of the $\pi^+ \pi^-$ pair is in the vicinity of the ω resonance. The sensitivity of the asymmetry, a , to N_c is small. Moreover, if N_c is constrained using the latest experimental branching ratios from the CLEO collaboration, we find that the sign of $\sin \delta$ is always positive. Thus, a measurement of direct CP violation in $B^\pm \rightarrow \rho^0 \pi^\pm$ would remove the $\text{mod}(\pi)$ ambiguity in $\arg \left[-\frac{V_{td} V_{tb}^*}{V_{ud} V_{ub}^*} \right]$.

PACS Numbers: 11.30.Er, 13.25.-Hw, 12.39.-x.

*xhguo@physics.adelaide.edu.au

†oleitner@physics.adelaide.edu.au

‡athomas@physics.adelaide.edu.au

1 Introduction

Even though CP violation has been known since 1964, we still do not know the source of CP violation clearly. In the Standard Model, a non-zero phase angle in the Cabbibo-Kobayashi-Maskawa (CKM) matrix is responsible for CP violating phenomena. In the past few years, numerous theoretical studies have been conducted on CP violation in the B meson system [1, 2]. However, we need a lot of data to check these approaches because there are many theoretical uncertainties – e.g. CKM matrix elements, hadronic matrix elements and nonfactorizable effects. The future aim would be to reduce all these uncertainties.

Direct CP violating asymmetries in B decays occur through the interference of at least two amplitudes with different weak phase ϕ and strong phase δ . In order to extract the weak phase (which is determined by the CKM matrix elements), one must know the strong phase δ and this is usually not well determined. In addition, in order to have a large signal, we have to appeal to some phenomenological mechanism to obtain a large δ . The charge symmetry violating mixing between ρ^0 and ω , can be extremely important in this regard. In particular, it can lead to a large CP violation in B decays such as $B^\pm \rightarrow \rho^0(\omega)\pi^\pm \rightarrow \pi^+\pi^-\pi^\pm$, because the strong phase passes through 90° at the ω resonance [3, 4, 5]. Recently, CLEO reported new data [6] on $B \rightarrow \rho\pi$. It is the aim of the present work to analyse direct CP violation in $B^\pm \rightarrow \rho^0(\omega)\pi^\pm \rightarrow \pi^+\pi^-\pi^\pm$, including $\rho-\omega$ mixing, using the latest data from the CLEO collaboration to constrain the calculation. In order to extract the strong phase δ , we use the factorization approach, in which the hadronic matrix elements of operators are saturated by vacuum intermediate states.

In this paper, we investigate five phenomenological models with different weak form factors and determine the CP violating asymmetry for $B^\pm \rightarrow \rho^0(\omega)\pi^\pm \rightarrow \pi^+\pi^-\pi^\pm$ in these models. We select models which are consistent with the CLEO data and determine the allowed range of N_c ($0.98(0.94) < N_c < 2.01(1.95)$). Then, we study the sign of $\sin \delta$ in the range of N_c allowed by experimental data in all these models. We discuss the model dependence of our results in detail.

The remainder of this paper is organized as follows. In Section 2, we present the form of the effective Hamiltonian and the values of Wilson coefficients. In Section 3, we give the formalism for the CP violating asymmetry in $B^+ \rightarrow \rho^0(\omega)\pi^+ \rightarrow \pi^+\pi^-\pi^+$, for all the models which will be checked. We also show numerical results in this section (asymmetry, a , the value of $\sin \delta$). In Section 4, we calculate branching ratios for $B^+ \rightarrow \rho^0\pi^+$ and $B^0 \rightarrow \rho^+\pi^-$ and present numerical results over the range of N_c allowed by the CLEO data. In last section, we summarize our results and suggest further work.

2 The effective Hamiltonian

In order to calculate the direct CP violating asymmetry in hadronic decays, one can use the following effective weak Hamiltonian, based on the operator product expansion [7],

$$\mathcal{H}_{\Delta B=1} = \frac{G_F}{\sqrt{2}} \left[\sum_{q=d,s} V_{ub}V_{uq}^* (c_1 O_1^u + c_2 O_2^u) - V_{tb}V_{tq}^* \sum_{i=3}^{10} c_i O_i \right] + h.c., \quad (1)$$

where $c_i (i = 1, \dots, 10)$ are the Wilson coefficients. They are calculable in renormalization group improved perturbation theory and are scale dependent. In the present case, we use

their values at the renormalization scale $\mu \approx m_b$. The operators O_i have the following form,

$$\begin{aligned}
O_1^u &= \bar{q}_\alpha \gamma_\mu (1 - \gamma_5) u_\beta \bar{u}_\beta \gamma^\mu (1 - \gamma_5) b_\alpha, & O_2^u &= \bar{q} \gamma_\mu (1 - \gamma_5) u \bar{u} \gamma^\mu (1 - \gamma_5) b, \\
O_3 &= \bar{q} \gamma_\mu (1 - \gamma_5) b \sum_{q'} \bar{q}' \gamma^\mu (1 - \gamma_5) q', & O_4 &= \bar{q}_\alpha \gamma_\mu (1 - \gamma_5) b_\beta \sum_{q'} \bar{q}'_\beta \gamma^\mu (1 - \gamma_5) q'_\alpha, \\
O_5 &= \bar{q} \gamma_\mu (1 - \gamma_5) b \sum_{q'} \bar{q}' \gamma^\mu (1 + \gamma_5) q', & O_6 &= \bar{q}_\alpha \gamma_\mu (1 - \gamma_5) b_\beta \sum_{q'} \bar{q}'_\beta \gamma^\mu (1 + \gamma_5) q'_\alpha, \\
O_7 &= \frac{3}{2} \bar{q} \gamma_\mu (1 - \gamma_5) b \sum_{q'} e_{q'} \bar{q}' \gamma^\mu (1 + \gamma_5) q', \\
O_8 &= \frac{3}{2} \bar{q}_\alpha \gamma_\mu (1 - \gamma_5) b_\beta \sum_{q'} e_{q'} \bar{q}'_\beta \gamma^\mu (1 + \gamma_5) q'_\alpha, \\
O_9 &= \frac{3}{2} \bar{q} \gamma_\mu (1 - \gamma_5) b \sum_{q'} e_{q'} \bar{q}' \gamma^\mu (1 - \gamma_5) q', \\
O_{10} &= \frac{3}{2} \bar{q}_\alpha \gamma_\mu (1 - \gamma_5) b_\beta \sum_{q'} e_{q'} \bar{q}'_\beta \gamma^\mu (1 - \gamma_5) q'_\alpha, \tag{2}
\end{aligned}$$

where α and β are color indices, and $q' = u, d$ or s quarks. In Eq.(2), O_1 and O_2 are the tree level operators, $O_3 - O_6$ are QCD penguin operators, and $O_7 - O_{10}$ arise from electroweak penguin diagrams.

The Wilson coefficients, c_i , are known to the next-to-leading logarithmic order. At the scale $\mu = m_b = 5\text{GeV}$, they take values the following values [8, 9]:

$$\begin{aligned}
c_1 &= -0.3125, & c_2 &= 1.1502, \\
c_3 &= 0.0174, & c_4 &= -0.0373, \\
c_5 &= 0.0104, & c_6 &= -0.0459, \\
c_7 &= -1.050 \times 10^{-5}, & c_8 &= 3.839 \times 10^{-4}, \\
c_9 &= -0.0101, & c_{10} &= 1.959 \times 10^{-3}. \tag{3}
\end{aligned}$$

To be consistent, the matrix elements of the operators O_i should also be renormalized to the one-loop order. This results in the effective Wilson coefficients, c'_i , which satisfy the constraint,

$$c_i(m_b)\langle O_i(m_b)\rangle = c'_i\langle O_i\rangle^{tree}, \quad (4)$$

where $\langle O_i\rangle^{tree}$ are the matrix elements at the tree level, which will be evaluated in the factorization approach. From Eq.(4), the relations between c'_i and c_i are [8, 9],

$$\begin{aligned} c'_1 &= c_1, & c'_2 &= c_2, \\ c'_3 &= c_3 - P_s/3, & c'_4 &= c_4 + P_s, \\ c'_5 &= c_5 - P_s/3, & c'_6 &= c_6 + P_s, \\ c'_7 &= c_7 + P_e, & c'_8 &= c_8, \\ c'_9 &= c_9 + P_e, & c'_{10} &= c_{10}, \end{aligned} \quad (5)$$

where

$$\begin{aligned} P_s &= (\alpha_s/8\pi)c_2(10/9 + G(m_c, \mu, q^2)), \\ P_e &= (\alpha_{em}/9\pi)(3c_1 + c_2)(10/9 + G(m_c, \mu, q^2)), \end{aligned}$$

with

$$G(m_c, \mu, q^2) = 4 \int_0^1 dx x(x-1) \ln \frac{m_c^2 - x(1-x)q^2}{\mu^2}.$$

Here q^2 is the typical momentum transfer of the gluon or photon in the penguin diagrams.

$G(m_c, \mu, q^2)$ has the following explicit expression [10],

$$\begin{aligned}\Re G &= \frac{2}{3} \left(\ln \frac{m_c^2}{\mu^2} - \frac{5}{3} - 4 \frac{m_c^2}{q^2} + \left(1 + 2 \frac{m_c^2}{q^2} \right) \sqrt{1 - 4 \frac{m_c^2}{q^2}} \ln \frac{1 + \sqrt{1 - 4 \frac{m_c^2}{q^2}}}{1 - \sqrt{1 - 4 \frac{m_c^2}{q^2}}} \right), \\ \Im m G &= -\frac{2}{3} \left(1 + 2 \frac{m_c^2}{q^2} \right) \sqrt{1 - 4 \frac{m_c^2}{q^2}}.\end{aligned}\quad (6)$$

Based on simple arguments at the quark level, the value of q^2 is chosen in the range $0.3 < q^2/m_b^2 < 0.5$ [3, 4]. From Eqs.(5,6) we can obtain numerical values for c'_i .

When $q^2/m_b^2 = 0.3$,

$$\begin{aligned}c'_1 &= -0.3125, & c'_2 &= 1.1502, \\ c'_3 &= 2.433 \times 10^{-2} + 1.543 \times 10^{-3}i, & c'_4 &= -5.808 \times 10^{-2} - 4.628 \times 10^{-3}i, \\ c'_5 &= 1.733 \times 10^{-2} + 1.543 \times 10^{-3}i, & c'_6 &= -6.668 \times 10^{-2} - 4.628 \times 10^{-3}i, \\ c'_7 &= -1.435 \times 10^{-4} - 2.963 \times 10^{-5}i, & c'_8 &= 3.839 \times 10^{-4}, \\ c'_9 &= -1.023 \times 10^{-2} - 2.963 \times 10^{-5}i, & c'_{10} &= 1.959 \times 10^{-3},\end{aligned}\quad (7)$$

and when $q^2/m_b^2 = 0.5$, one has,

$$\begin{aligned}c'_1 &= -0.3125, & c'_2 &= 1.1502, \\ c'_3 &= 2.120 \times 10^{-2} + 2.174 \times 10^{-3}i, & c'_4 &= -4.869 \times 10^{-2} - 1.552 \times 10^{-2}i, \\ c'_5 &= 1.420 \times 10^{-2} + 5.174 \times 10^{-3}i, & c'_6 &= -5.729 \times 10^{-2} - 1.552 \times 10^{-2}i, \\ c'_7 &= -8.340 \times 10^{-5} - 9.938 \times 10^{-5}i, & c'_8 &= 3.839 \times 10^{-4}, \\ c'_9 &= -1.017 \times 10^{-2} - 9.938 \times 10^{-5}i, & c'_{10} &= 1.959 \times 10^{-3},\end{aligned}\quad (8)$$

where we have taken $\alpha_s(m_Z) = 0.112$, $\alpha_{em}(m_b) = 1/132.2$, $m_b = 5\text{GeV}$, and $m_c = 1.35\text{GeV}$.

3 CP violation in $B^+ \rightarrow \rho^0(\omega)\pi^+ \rightarrow \pi^+\pi^-\pi^+$

3.1 Formalism

The formalism for CP violation in hadronic B meson decays is the following. Let A be the amplitude for the decay $B^+ \rightarrow \pi^+\pi^-\pi^+$, then one has

$$A = \langle \pi^+\pi^-\pi^+ | H^T | B^+ \rangle + \langle \pi^+\pi^-\pi^+ | H^P | B^+ \rangle, \quad (9)$$

with H^T and H^P being the Hamiltonians for the tree and penguin operators, respectively.

We can define the relative magnitude and phases between these two contributions as follows,

$$A = \langle \pi^+\pi^-\pi^+ | H^T | B^+ \rangle [1 + r e^{i\delta} e^{i\phi}], \quad (10)$$

$$\bar{A} = \langle \pi^+\pi^-\pi^- | H^T | B^- \rangle [1 + r e^{i\delta} e^{-i\phi}], \quad (11)$$

where δ and ϕ are strong and weak phases, respectively. The phase ϕ arises from the appropriate combination of CKM matrix elements which is $\phi = \arg[(V_{tb}V_{td}^*)/(V_{ub}V_{ud}^*)]$.

As a result, $\sin \phi$ is equal to $\sin \alpha$ with α defined in the standard way [11]. The parameter r is the absolute value of the ratio of tree and penguin amplitudes:

$$r \equiv \left| \frac{\langle \rho^0(\omega)\pi^+ | H^P | B^+ \rangle}{\langle \rho^0(\omega)\pi^+ | H^T | B^+ \rangle} \right|. \quad (12)$$

The CP violating asymmetry, a , can be written as:

$$a \equiv \frac{|A|^2 - |\bar{A}|^2}{|A|^2 + |\bar{A}|^2} = \frac{-2r \sin \delta \sin \phi}{1 + 2r \cos \delta \cos \phi + r^2}. \quad (13)$$

It can be seen explicitly from Eq.(13) that both weak and strong phase differences are needed to produce CP violation. In order to obtain a large signal for direct CP violation, we need some mechanism to make both $\sin \delta$ and r large. We stress that $\rho - \omega$ mixing has the dual advantages that the strong phase difference is large (passing through 90° at the ω resonance) and well known [4, 5]. With this mechanism, to first order in isospin violation, we have the following results when the invariant mass of $\pi^+\pi^-$ is near the ω resonance mass,

$$\langle \pi^-\pi^+\pi^+ | H^T | B^+ \rangle = \frac{g_\rho}{s_\rho s_\omega} \tilde{\Pi}_{\rho\omega} t_\omega + \frac{g_\rho}{s_\rho} t_\rho, \quad (14)$$

$$\langle \pi^-\pi^+\pi^+ | H^P | B^+ \rangle = \frac{g_\rho}{s_\rho s_\omega} \tilde{\Pi}_{\rho\omega} p_\omega + \frac{g_\rho}{s_\rho} p_\rho. \quad (15)$$

Here $t_V(V = \rho \text{ or } \omega)$ is the tree amplitude and p_V the penguin amplitude for producing a vector meson, V , g_ρ is the coupling for $\rho^0 \rightarrow \pi^+\pi^-$, $\tilde{\Pi}_{\rho\omega}$ is the effective $\rho - \omega$ mixing amplitude, and s_V is from the inverse propagator of the vector meson V ,

$$s_V = s - m_V^2 + im_V\Gamma_V, \quad (16)$$

with \sqrt{s} being the invariant mass of the $\pi^+\pi^-$ pair.

We stress that the direct coupling $\omega \rightarrow \pi^+\pi^-$ is effectively absorbed into $\tilde{\Pi}_{\rho\omega}$ [12], leading to the explicit s dependence of $\tilde{\Pi}_{\rho\omega}$. Making the expansion $\tilde{\Pi}_{\rho\omega}(s) = \tilde{\Pi}_{\rho\omega}(m_\omega^2) + (s - m_\omega^2)\tilde{\Pi}'_{\rho\omega}(m_\omega^2)$, the $\rho - \omega$ mixing parameters were determined in the fit of Gardner and O'Connell [13]: $\Re e \tilde{\Pi}_{\rho\omega}(m_\omega^2) = -3500 \pm 300 \text{MeV}^2$, $\Im m \tilde{\Pi}_{\rho\omega}(m_\omega^2) = -300 \pm 300 \text{MeV}^2$ and $\tilde{\Pi}'_{\rho\omega}(m_\omega^2) = 0.03 \pm 0.04$. In practice, the effect of the derivative term is negligible. From Eqs.(10,14,15) one has,

$$r e^{i\delta} e^{i\phi} = \frac{\tilde{\Pi}_{\rho\omega} p_\omega + s_\omega p_\rho}{\tilde{\Pi}_{\rho\omega} t_\omega + s_\omega t_\rho}. \quad (17)$$

Defining

$$\frac{p_\omega}{t_\rho} \equiv r' e^{i(\delta_q + \phi)}, \quad \frac{t_\omega}{t_\rho} \equiv \alpha e^{i\delta_\alpha}, \quad \frac{p_\rho}{p_\omega} \equiv \beta e^{i\delta_\beta}, \quad (18)$$

where $\delta_\alpha, \delta_\beta$ and δ_q are strong phases, one finds the following expression from Eq.(18)

$$r e^{i\delta} = r' e^{i\delta_q} \frac{\tilde{\Pi}_{\rho\omega} + \beta e^{i\delta_\beta} s_\omega}{s_\omega + \tilde{\Pi}_{\rho\omega} \alpha e^{i\delta_\alpha}}. \quad (19)$$

It will be shown that in the factorization approach, we have $\alpha e^{i\delta_\alpha} = 1$ in our case. Letting

$$\beta e^{i\delta_\beta} = b + ci, \quad r' e^{i\delta_q} = d + ei, \quad (20)$$

and using Eq.(20), we obtain the following result when $\sqrt{s} \sim m_\omega$

$$r e^{i\delta} = \frac{C + Di}{(s - m_\omega^2 + \Re \tilde{\Pi}_{\rho\omega})^2 + (\Im \tilde{\Pi}_{\rho\omega} + m_\omega \Gamma_\omega)^2}, \quad (21)$$

where

$$\begin{aligned} C &= (s - m_\omega^2 + \Re \tilde{\Pi}_{\rho\omega}) \left\{ d[\Re \tilde{\Pi}_{\rho\omega} + b(s - m_\omega^2) - cm_\omega \Gamma_\omega] \right. \\ &\quad \left. - e[\Im \tilde{\Pi}_{\rho\omega} + bm_\omega \Gamma_\omega + c(s - m_\omega^2)] \right\} \\ &\quad + (\Im \tilde{\Pi}_{\rho\omega} + m_\omega \Gamma_\omega) \left\{ e[\Re \tilde{\Pi}_{\rho\omega} + b(s - m_\omega^2) - cm_\omega \Gamma_\omega] \right. \\ &\quad \left. + d[\Im \tilde{\Pi}_{\rho\omega} + bm_\omega \Gamma_\omega + c(s - m_\omega^2)] \right\}, \\ D &= (s - m_\omega^2 + \Re \tilde{\Pi}_{\rho\omega}) \left\{ e[\Re \tilde{\Pi}_{\rho\omega} + d(s - m_\omega^2) - cm_\omega \Gamma_\omega] \right. \\ &\quad \left. + d[\Im \tilde{\Pi}_{\rho\omega} + bm_\omega \Gamma_\omega + c(s - m_\omega^2)] \right\} \\ &\quad - (\Im \tilde{\Pi}_{\rho\omega} + m_\omega \Gamma_\omega) \left\{ d[\Re \tilde{\Pi}_{\rho\omega} + b(s - m_\omega^2) - cm_\omega \Gamma_\omega] \right. \\ &\quad \left. - e[\Im \tilde{\Pi}_{\rho\omega} + bm_\omega \Gamma_\omega + c(s - m_\omega^2)] \right\}. \end{aligned} \quad (22)$$

$\beta e^{i\delta_\beta}$ and $r' e^{i\delta_q}$ will be calculated later. Then, from Eq.(22) we can obtain $r \sin \delta$ and $r \cos \delta$. In order to get the CP violating asymmetry, a , in Eq.(13), $\sin \phi$ and $\cos \phi$ are needed, where ϕ is determined by the CKM matrix elements. In the Wolfenstein parametrization [14], one has,

$$\sin \phi = \frac{\eta}{\sqrt{[\rho(1-\rho) - \eta^2]^2 + \eta^2}}, \quad (23)$$

$$\cos \phi = \frac{\rho(1-\rho) - \eta^2}{\sqrt{[\rho(1-\rho) - \eta^2]^2 + \eta^2}}. \quad (24)$$

3.2 Computational Details

With the Hamiltonian given in Eq.(1), we are ready to evaluate the matrix elements for $B^+ \rightarrow \rho^0(\omega)\pi^+$. In the factorization approximation, either the $\rho^0(\omega)$ or the π^+ is generated by one current which has the appropriate quantum numbers in the Hamiltonian. For this decay process, two kinds of matrix element products are involved after factorization; schematically (i.e. omitting Dirac matrices and color labels) $\langle \rho^0(\omega)|(\bar{u}u)|0\rangle\langle \pi^+|(\bar{d}b)|B^+\rangle$ and $\langle \pi^+|(\bar{d}u)|0\rangle\langle \rho^0(\omega)|(\bar{u}b)|B^+\rangle$. We will calculate them in some phenomenological quark models.

The matrix elements for $B \rightarrow X$ and $B \rightarrow X^*$ (where X and X^* denote pseudoscalar and vector mesons, respectively) can be decomposed as [15],

$$\langle X|J_\mu|B\rangle = \left(p_B + p_X - \frac{m_B^2 - m_X^2}{k^2}k\right)_\mu F_1(k^2) + \frac{m_B^2 - m_X^2}{k^2}k_\mu F_0(k^2), \quad (25)$$

$$\begin{aligned} \langle X^*|J_\mu|B\rangle &= \frac{2}{m_B + m_{X^*}}\epsilon_{\mu\nu\rho\sigma}\epsilon^{*\nu}p_B^\rho p_{X^*}^\sigma V(k^2) + i\{\epsilon_\mu^*(m_B + m_{X^*})A_1(k^2) \\ &\quad - \frac{\epsilon^* \cdot k}{m_B + m_{X^*}}(P_B + P_{X^*})_\mu A_2(k^2) - \frac{\epsilon^* \cdot k}{k^2}2m_{X^*} \cdot k_\mu A_3(k^2)\} \\ &\quad + i\frac{\epsilon^* \cdot k}{k^2}2m_{X^*} \cdot k_\mu A_0(k^2), \end{aligned} \quad (26)$$

where J_μ is the weak current ($J_\mu = \bar{q}\gamma^\mu(1 - \gamma_5)b$ with $q = u, d$), $k = p_B - p_{X(X^*)}$ and ϵ_μ is the polarization vector of X^* . The form factors included in our calculations satisfy: $F_1(0) = F_0(0)$, $A_3(0) = A_0(0)$ and $A_3(k^2) = \frac{m_B+m_{X^*}}{2m_{X^*}}A_1(k^2) - \frac{m_B-m_{X^*}}{2m_{X^*}}A_2(k^2)$. Using the decomposition in Eqs.(25, 26), one has,

$$t_\rho = m_B|\vec{p}_\rho| \left[\left(c'_1 + \frac{1}{N_c}c'_2 \right) f_\rho F_1(m_\rho^2) + \left(c'_2 + \frac{1}{N_c}c'_1 \right) f_\pi A_0(m_\pi^2) \right], \quad (27)$$

where f_ρ and f_π are the decay constants of the ρ and π , respectively, and \vec{p}_ρ is the three momentum of the ρ . In the same way, we find $t_\omega = t_\rho$, so that

$$\alpha e^{i\delta_\alpha} = 1. \quad (28)$$

After calculating the penguin operator contributions, one has,

$$\begin{aligned} \beta e^{i\delta_\beta} = \frac{m_B|\vec{p}_\rho|}{p_\omega} & \left\{ \left(c'_4 + \frac{1}{N_c}c'_3 \right) [-f_\rho F_1(m_\rho^2) + f_\pi A_0(m_\pi^2)] \right. \\ & + \frac{3}{2} \left[\left(c'_7 + \frac{1}{N_c}c'_8 \right) + \left(c'_9 + \frac{1}{N_c}c'_{10} \right) \right] f_\rho F_1(m_\rho^2) \\ & - \left[\left(c'_6 + \frac{1}{N_c}c'_5 \right) + \left(c'_8 + \frac{1}{N_c}c'_7 \right) \right] \left[\frac{2m_\pi^2 f_\pi A_0(m_\pi^2)}{(m_u + m_d)(m_b + m_u)} \right] \\ & \left. + \left(c'_{10} + \frac{1}{N_c}c'_9 \right) \left[\frac{1}{2} f_\rho F_1(m_\rho^2) + f_\pi A_0(m_\pi^2) \right] \right\}, \\ r' e^{i\delta_q} = & - \frac{p_\omega}{\left(c'_1 + \frac{1}{N_c}c'_2 \right) f_\rho F_1(m_\rho^2) + \left(c'_2 + \frac{1}{N_c}c'_1 \right) f_\pi A_0(m_\pi^2)} \left| \frac{V_{tb}V_{td}^*}{V_{ub}V_{ud}^*} \right|, \end{aligned} \quad (29)$$

where

$$p_\omega = m_B|\vec{p}_\rho| \left\{ 2 \left[\left(c'_3 + \frac{1}{N_c}c'_4 \right) + \left(c'_5 + \frac{1}{N_c}c'_6 \right) \right] f_\rho F_1(m_\rho^2) \right.$$

$$\begin{aligned}
& +\frac{1}{2} \left[(c'_7 + \frac{1}{N_c} c'_8) + (c'_9 + \frac{1}{N_c} c'_{10}) \right] f_\rho F_1(m_\rho^2) \\
& -2 \left[(c'_8 + \frac{1}{N_c} c'_7) + (c'_6 + \frac{1}{N_c} c'_5) \right] \left[\frac{m_\pi^2 f_\pi A_0(m_\pi^2)}{(m_u + m_d)(m_b + m_u)} \right] \\
& + (c'_4 + \frac{1}{N_c} c'_3) \left[f_\pi A_0(m_\pi^2) + f_\rho F_1(m_\rho^2) \right] \\
& + (c'_{10} + \frac{1}{N_c} c'_9) \left[f_\pi A_0(m_\pi^2) - \frac{1}{2} f_\rho F_1(m_\rho^2) \right] \Big\},
\end{aligned}$$

and

$$\left| \frac{V_{tb} V_{td}^*}{V_{ub} V_{ud}^*} \right| = \frac{\sqrt{(1-\rho)^2 + \eta^2}}{(1-\lambda^2/2)\sqrt{\rho^2 + \eta^2}} = \left(1 - \frac{\lambda^2}{2}\right)^{-1} \left| \frac{\sin \gamma}{\sin \beta} \right|. \quad (30)$$

3.3 Numerical Results

In our numerical calculations we have several parameters: q^2 , N_c and the CKM matrix elements in the Wolfenstein parametrization. As mentioned in Section 2, the value of q^2 is conventionally chosen to be in the range $0.3 < q^2/m_b^2 < 0.5$. The CKM matrix, which should be determined from experimental data, has the following form in term of the Wolfenstein parameters, A , λ , ρ , η [14]:

$$V = \begin{pmatrix} 1 - \frac{1}{2}\lambda^2 & \lambda & A\lambda^3(\rho - i\eta) \\ -\lambda & 1 - \frac{1}{2}\lambda^2 & A\lambda^2 \\ A\lambda^3(1 - \rho - i\eta) & -A\lambda^2 & 1 \end{pmatrix}, \quad (31)$$

where $O(\lambda^4)$ corrections are neglected. We use $\lambda = 0.2205$, $A = 0.815$ and the range for ρ and η as the following [16, 17],

$$0.09 < \rho < 0.254, \quad 0.323 < \eta < 0.442. \quad (32)$$

The form factors $F_1(m_\rho^2)$ and $A_0(m_\pi^2)$ depend on the inner structure of the hadrons. Under the nearest pole dominance assumption, the k^2 dependence of the form factors is:

for model 1(2) [15, 18]:

$$F_1(k^2) = \frac{h_1}{1 - \frac{k^2}{m_1^2}}, \quad A_0(k^2) = \frac{h_{A_0}}{1 - \frac{k^2}{m_{A_0}^2}}, \quad (33)$$

where $h_1 = 0.330(0.625)$, $h_{A_0} = 0.28(0.34)$, $m_1 = 5.32\text{GeV}$, $m_{A_0} = 5.27\text{GeV}$,

for model 3(4) [15, 18, 19]:

$$F_1(k^2) = \frac{h_1}{\left(1 - \frac{k^2}{m_1^2}\right)^2}, \quad A_0(k^2) = \frac{h_{A_0}}{\left(1 - \frac{k^2}{m_{A_0}^2}\right)^2}, \quad (34)$$

where $h_1 = 0.330(0.625)$, $h_{A_0} = 0.28(0.34)$, $m_1 = 5.32\text{GeV}$, $m_{A_0} = 5.27\text{GeV}$,

for model 5 [20, 21]:

$$F_1(k^2) = \frac{h_1}{1 - a_1 \frac{k^2}{m_B^2} + b_1 \left(\frac{k^2}{m_B^2}\right)^2}, \quad A_0(k^2) = \frac{h_{A_0}}{1 - a_0 \frac{k^2}{m_B^2} + b_0 \left(\frac{k^2}{m_B^2}\right)^2}, \quad (35)$$

where $h_1 = 0.305$, $h_{A_0} = 0.372$, $a_1 = 0.266$, $b_1 = -0.752$, $a_0 = 1.4$, $b_0 = 0.437$.

The decay constants used in our calculations are: $f_\rho = f_\omega = 221\text{MeV}$ and $f_\pi = 130.7\text{MeV}$.

In the numerical calculations, it is found that for a fixed N_c , there is a maximum value, a_{max} , for the CP violating parameter, a , when the invariant mass of the $\pi^+\pi^-$ is in the vicinity of the ω resonance. The results are shown in Figs.1 and 2, for $k^2/m_b^2 = 0.3(0.5)$ and N_c in the range $0.98(0.94) < N_c < 2.01(1.95)$ – for reasons which will be explained later (Section 4). We investigate five models with different form factors to study the

model dependence of a . It appears that this dependence is strong (Table 1).

The maximum asymmetry parameter, a_{max} , varies from $-24\%(-19\%)$ to $-59\%(-48\%)$ for N_c in the chosen range, $k^2/m_b^2 = 0.3(0.5)$ and the range of CKM matrix elements indicated earlier. If we look at the numerical results for the asymmetries (Table 1) for $N_{cmax} = 2.01(1.95)$ and $k^2/m_b^2 = 0.3(0.5)$, we obtain for models 1, 3, 5 an asymmetry, a_{max} , around $-27.3\%(-21.6\%)$ for the set (ρ_{max}, η_{max}) , and around $-44.3\%(-35.0\%)$ for the set (ρ_{min}, η_{min}) . We find a ratio equal to 1.62(1.62) between the asymmetries associated with the upper and lower limits of (ρ, η) . The reason why the maximum asymmetry, a_{max} , can have large variation, comes from the $b \rightarrow d$ transition, where V_{td} and V_{ub} appear. These are functions of (ρ, η) and contribute to the asymmetry (Eq.31) through the ratio between the ω penguin diagram and the ρ tree diagram.

For models 2 and 4, one has a maximum asymmetry, a_{max} , around $-37\%(-28\%)$ for the set (ρ_{max}, η_{max}) and around $-59\%(-46\%)$ for the set (ρ_{min}, η_{min}) . We find a ratio between the asymmetries equal to 1.59(1.64) in this case. The difference between these two sets of models comes from the magnitudes of the form factors, where $F_1(k^2)$ is larger for models 2 and 4 than for models 1, 3 and 5. Now, if we look at the numerical results for the asymmetry for $N_{cmin} = 0.98(0.94)$, we find, for models 1, 3, 5, $k^2/m_b^2 = 0.3(0.5)$, and the set (ρ_{max}, η_{max}) , an asymmetry, a_{max} , around $-31.3\%(-25.6\%)$, and for the set (ρ_{min}, η_{min}) we find an asymmetry, a_{max} , around $-50.3\%(-42.0\%)$. In this case, one has a ratio equal to 1.61(1.64). Finally, for models 2 and 4, we get $-36\%(-29\%)$ for the set (ρ_{max}, η_{max}) and $-57\%(-48\%)$ for the set (ρ_{min}, η_{min}) with a ratio equal to 1.58(1.65).

These results show explicitly the dependence of the CP violating asymmetry on form factors, CKM matrix elements and the effective parameter N_c . For the CKM matrix

elements, it appears that if we take their upper limit, we obtain a smaller asymmetry, a , and viceversa. The difference between $k^2/m_b^2 = 0.3(0.5)$ in our results comes from the renormalization of the matrix elements of the operators in the weak Hamiltonian. Finally, the dependence on N_c comes from the fact that N_c is related to hadronization effects, and consequently we cannot determine N_c exactly in our calculations. Therefore, we treat N_c as a free effective parameter. As regards the ratio between the asymmetries, we have found a ratio equal to 1.61(1.63). This is mainly determined by the ratio $\sin \gamma / \sin \beta$, and more precisely by η . In Table 2, we show the values for the angles α , β , γ . From all these numerical results, we can conclude that we need to determine the value of N_c and the hadronic decay form factors more precisely, if we want to use the asymmetry, a , to constrain the CKM matrix elements.

In spite of the uncertainties just discussed, it is vital to realize that the effect of $\rho - \omega$ mixing in the $B \rightarrow \rho\pi$ decay is to remove any ambiguity concerning the strong phase, $\sin \delta$. As the internal top quark dominates the $b \rightarrow d$ transition, the weak phase in the rate asymmetry is proportional to $\sin \alpha$ ($= \sin \phi$), where $\alpha = \arg \left[-\frac{V_{td}V_{tb}^*}{V_{ud}V_{ub}^*} \right]$, and knowing the sign of $\sin \delta$ enables us to determine that of $\sin \alpha$ from a measurement of the asymmetry, a . We show in Fig.3 that the sign of $\sin \delta$ is always positive in our range, $0.98(0.94) < N_c < 2.01(1.95)$ for all the models studied. Indeed, at the $\pi^+\pi^-$ invariant mass where the asymmetry parameter, a , reaches a maximum, the value of $\sin \delta$ is equal to one – provided $\rho - \omega$ mixing is included – over the entire range of N_c and for all the form factors studied. So, we can remove, with the help of asymmetry, a , the uncertainty $\text{mod}(\pi)$ which appears in α from the usual indirect measurements [5] which yield $\sin 2\alpha$. By contrast, in the case where we do not take $\rho - \omega$ mixing into account, we find a small

value for $\sin \delta$. In Figs.3 and 4 we plot the role of $\rho - \omega$ mixing in our calculations. We stress that, even though one has a large value of $\sin \delta$ around $N_c = 1$ with no $\rho - \omega$ mixing, one still has a very small value for r (Fig.4), and hence the CP violating asymmetry, a , remains very small in that case.

4 Branching ratios for $B^+ \rightarrow \rho^0 \pi^+$ and $B^0 \rightarrow \rho^+ \pi^-$

4.1 Formalism

With the factorized decay amplitudes, we can compute the decay rates using by the following expression [19],

$$\Gamma(B \rightarrow VP) = \frac{|\vec{p}_\rho|^3}{8\pi m_V^2} \left| \frac{A(B \rightarrow VP)}{\epsilon \cdot p_B} \right|^2, \quad (36)$$

where

$$|\vec{p}_\rho| = \frac{\sqrt{[m_B^2 - (m_1 + m_2)^2][m_B^2 - (m_1 - m_2)^2]}}{2m_B} \quad (37)$$

is the c.m. momentum of the decay particles, $m_1(m_2)$ is the mass of the vector (pseudoscalar) V(P), and $A(B \rightarrow VP)$ is the decay amplitude:

$$A(B \rightarrow VP) = \frac{G_F}{\sqrt{2}} \sum_{i=1,10} V_u^{T,P} a_i \langle VP | O_i | B \rangle. \quad (38)$$

Here $V_u^{T,P}$ is CKM factor:

$$V_u^T = |V_{ub}V_{ud}^*| \quad \text{for } i = 1, 2 \quad \text{and} \quad V_u^P = |V_{tb}V_{td}^*| \quad \text{for } i = 3, \dots, 10$$

where the effective parameters are the following combinations

$$a_{2j} = c'_{2j} + \frac{1}{N_c}c'_{2j-1}, \quad a_{2j-1} = c'_{2j-1} + \frac{1}{N_c}c'_{2j}, \quad \text{for } j = 1, \dots, 5$$

and $\langle VP|O_i|B \rangle$ is a matrix element which is evaluated in the factorization approach.

In the Quark Model, the diagram coming from the $B^+ \rightarrow \rho^0\pi^+$ decay is the only one contribution. In our case, to be consistent, we should also take into account the $\rho - \omega$ mixing contribution when we calculate the branching ratio since we are working to the first order of isospin violation. Explicitly, we obtain for $B^+ \rightarrow \rho^0\pi^+$,

$$\begin{aligned} BR(B^+ \rightarrow \rho^0\pi^+) &= \frac{G_F^2 |\vec{p}_\rho|^3}{32\pi\Gamma_{B^+}} \left| \left[V_u^T A_{\rho^0}^T(a_1, a_2) - V_u^P A_{\rho^0}^P(a_3, \dots, a_{10}) \right] \right. \\ &\quad \left. + \left[V_u^T A_\omega^T(a_1, a_2) - V_u^P A_\omega^P(a_3, \dots, a_{10}) \right] \frac{\tilde{\Pi}_{\rho\omega}}{(s_\rho - m_\omega^2) + im_\omega\Gamma_\omega} \right|^2, \end{aligned} \quad (39)$$

where the tree and penguin amplitudes are:

$$\begin{aligned} \sqrt{2}A_{\rho^0}^T(a_1, a_2) &= a_1 f_\rho F_1(m_\rho^2) + a_2 f_\pi A_0(m_\pi^2), \\ \sqrt{2}A_{\rho^0}^P(a_3, \dots, a_{10}) &= a_4 \left[-f_\rho F_1(m_\rho^2) + f_\pi A_0(m_\pi^2) \right] + a_{10} \left[\frac{1}{2} f_\rho F_1(m_\rho^2) + f_\pi A_0(m_\pi^2) \right] \\ &\quad + \frac{3}{2}(a_7 + a_9) f_\rho F_1(m_\rho^2) - 2(a_6 + a_8) \left[\frac{m_\pi^2 f_\pi A_0(m_\pi^2)}{(m_u + m_d)(m_b + m_u)} \right], \\ \sqrt{2}A_\omega^T(a_1, a_2) &= a_1 f_\rho F_1(m_\rho^2) + a_2 f_\pi A_0(m_\pi^2), \end{aligned}$$

$$\begin{aligned}
\sqrt{2}A_\omega^P(a_3, \dots, a_{10}) &= \left[2(a_3 + a_5) + \frac{1}{2}(a_7 + a_9) \right] f_\rho F_1(m_\rho^2) \\
&\quad - 2(a_8 + a_6) \left[\frac{m_\pi^2 f_\pi A_0(m_\pi^2)}{(m_u + m_d)(m_b + m_u)} \right] \\
&\quad + a_4 \left[f_\pi A_0(m_\pi^2) + f_\rho F_1(m_\rho^2) \right] + a_{10} \left[f_\pi A_0(m_\pi^2) - \frac{1}{2}f_\rho F_1(m_\rho^2) \right],
\end{aligned}$$

where $\langle \rho^0 | \bar{u}u | 0 \rangle = \frac{1}{\sqrt{2}} f_\rho m_\rho \epsilon_\rho$ and $\langle \pi^+ | \bar{u}d | 0 \rangle = i f_\pi p_\mu$.

For $B^0 \rightarrow \rho^+ \pi^-$ we obtain,

$$BR(B^0 \rightarrow \rho^+ \pi^-) = \frac{G_F^2 |\vec{p}_\rho|^3}{16\pi\Gamma_{B^0}} \left| V_u^T A_{\rho^+}^T(a_2) - V_u^P A_{\rho^+}^P(a_3, \dots, a_{10}) \right|^2, \quad (40)$$

where

$$A_{\rho^+}^T(a_2) = a_2 f_\rho F_1(m_\rho^2),$$

$$A_{\rho^+}^P(a_3, \dots, a_{10}) = (a_4 + a_{10}) f_\rho F_1(m_\rho^2).$$

Moreover, we can calculate the ratio between these two branching ratios, in which the uncertainty caused by many systematic errors is removed. We define the ratio R as:

$$R = \frac{BR(B^0 \rightarrow \rho^+ \pi^-)}{BR(B^+ \rightarrow \rho^0 \pi^+)}, \quad (41)$$

and, without taking into account the penguin contribution, one has,

$$R = \frac{2\Gamma_{B^+}}{\Gamma_{B^0}} \left| \left(\frac{a_1}{a_2} + \frac{f_\pi A_0(m_\pi^2)}{f_\rho F_1(m_\rho^2)} \right) \left(1 + \frac{\tilde{\Pi}_{\rho\omega}}{(s_\rho - m_\omega^2) + im_\omega\Gamma_\omega} \right) \right|^{-2} \quad (42)$$

4.2 Numerical Results

The latest experimental data from the CLEO collaboration [6] are:

$$BR(B^+ \rightarrow \rho^0 \pi^+) = (10.4_{-3.4}^{+3.3} \pm 2.1) \times 10^{-6},$$

$$BR(B^0 \rightarrow \rho^+ \pi^-) = (27.6_{-7.4}^{+8.4} \pm 4.2) \times 10^{-6},$$

$$R = 2.65 \pm 1.9.$$

We have calculated the branching ratios for $B^0 \rightarrow \rho^+ \pi^-$ and for $B^+ \rightarrow \rho^0 \pi^+$ for all models as a function of N_c . In Figs.5 and 6, we show the results for models 1 and 2 in order to make the dependence on form factors explicit.

The numerical results are very sensitive to uncertainties coming from the experimental data. For the branching ratio $B^0 \rightarrow \rho^+ \pi^-$ (Fig.5), we have a large range of values of N_c and the CKM matrix elements over which the theoretical results are consistent with the experimental data from CLEO. However, all models do not give the same result: models 2 and 4 are very close to the experimental data for a large range of N_c , whereas models 1,3 and 5 are not. The reason is still the magnitude of the form factors. As a result, we have to exclude models 1,3 and 5 because their form factors are too small.

If we consider numerical results for branching ratio $B^+ \rightarrow \rho^0 \pi^+$ (Fig.6), it appears that all models are consistent with the experimental data for a large range of N_c . The effect of $\rho - \omega$ mixing (included in our calculations) on the branching ratio $B^+ \rightarrow \rho^0 \pi^+$ is around 30%. Numerical results for models 1, 3, 5 and models 2, 4 are very close to each other. The difference between the two branching ratios can be explained by the fact that for the $B^0 \rightarrow \rho^+ \pi^-$ decay, the tree and penguin contributions are both proportional to only

one form factor, $F_1(k^2)$. Thus, this branching ratio is very sensitive to the magnitude of this form factor ($F_1(k^2)$ is related to $h_1 = 0.330$ or 0.625 in models (1,3) and (2,4) respectively). On the other hand, for the decay $B^+ \rightarrow \rho^0 \pi^+$, both $F_1(k^2)$ and $A_0(k^2)$ are included in the tree and penguin amplitudes, and this branching ratio is less sensitive to the magnitude of the form factors.

If we look at the ratio R between these two branching ratios, $BR(B^+ \rightarrow \rho^0 \pi^+)$ and $BR(B^0 \rightarrow \rho^+ \pi^-)$ – shown in Fig.7 – the results indicate that R is very sensitive to the magnitude of the form factors, and that there is a large difference between models 1, 3, 5 and models 2 and 4. We investigated the ratio R for the limiting CKM matrix elements as a function of N_c , finding that R is consistent with the experimental data over the range N_c : $0.98(0.94) < N_c < 2.01(1.95)$, (The values outside(inside) brackets correspond to the choice $q^2/m_b^2 = 0.3(0.5)$). It should be noted that R , in particular, is not very sensitive to the CKM matrix elements. The small difference which does appear, comes from the penguin contributions (which may be neglected). If we just take into account the tree contributions in our calculations, R is clearly independent of the CKM matrix elements (Eq.42).

From a comparison of the numerical results and the experimental data, we can extract a range of N_c , within which all results are consistent. In Table 3, we have summarized the allowed range of N_c for $B^+ \rightarrow \rho^0 \pi^+$, $B^0 \rightarrow \rho^+ \pi^-$ and R , for models 1, 2, 3, 4 and 5 according to various choices of the CKM matrix elements. To determine the best range of N_c , we have to find some intersection of the values of N_c for each model and for each set of CKM matrix elements, for which the theoretical and experimental results are consistent. This is possible and the results are shown in Table 4. In our study, it seems better to use

the range intersection $\{N_c\}_{B^+} \cap \{N_c\}_R$ than $\{N_c\}_{B^0} \cap \{N_c\}_{B^+}$, for fixing the final interval N_c , since the experimental uncertainties are smaller in the former case, and since we are working to the first order of isospin violation ($\rho - \omega$ mixing). Finally, after excluding models 1,3 and 5, which are not consistent with all the experimental data, we are able to fix the upper and lower limit of the range of N_c , using the limiting values of the CKM matrix elements (Table 5). We find that N_c should be in the range $0.98(0.94) < N_c < 2.01(1.95)$ where N_{cmin} and N_{cmax} correspond to (ρ_{min}, η_{min}) and (ρ_{max}, η_{max}) respectively.

5 Summary and discussion

The first aim of the present work was to compare our theoretical results with the latest experimental data from the CLEO collaboration for the branching ratios $B^+ \rightarrow \rho^0 \pi^+$ and $B^0 \rightarrow \rho^+ \pi^-$. Our next aim was to study direct CP violation for the decay $B^+ \rightarrow \rho^0(\omega) \pi^+ \rightarrow \pi^+ \pi^- \pi^+$, with the inclusion of $\rho - \omega$ mixing. The advantage of $\rho - \omega$ mixing is that the strong phase difference is large and rapidly varying near the ω resonance. As a result the CP violating asymmetry, a , has a maximum, a_{max} , when the invariant mass of the $\pi^+ \pi^-$ pair is in the vicinity of the ω resonance and $\sin \delta = +1$ at this point.

In the calculation of CP violating asymmetry parameters, we need the Wilson coefficients for the tree and penguin operators at the scale m_b . We worked with the renormalization scheme independent Wilson coefficients. One of the major uncertainties is that the hadronic matrix elements for both tree and penguin operators involve nonperturbative QCD. We have worked in the factorization approximation, with N_c treated as an effective parameter. Although one must have some doubts about factorization, it has been pointed

out that it may be quite reliable in energetic weak decays [22, 23].

We have explicitly shown that the CP violating asymmetry, a , is very sensitive to the CKM matrix elements and the magnitude of the form factors, and we have determined a range for the maximum asymmetry, a_{max} , as a function of the parameter N_c , the limits of CKM matrix elements and the choice of $k^2/m_b^2 = 0.3(0.5)$. From all the models investigated, we found that CP violating asymmetry, a_{max} , varies from $-24\%(-19\%)$ to $-59\%(-48\%)$. We stressed that the ratio between the asymmetries associated with the limiting values of CKM matrix elements would be mainly determined by η . Moreover, we also stressed that without $\rho - \omega$ mixing, we cannot have a large CP violating asymmetry, a , since a is proportional to both $\sin \delta$ and r . Even though $\sin \delta$ is large around $N_c = 1$, r is very small. As a result, we find a very small value for the CP violation in the decay $B^\pm \rightarrow \rho^0 \pi^\pm$ (of the order of a few percent) without mixing. Once mixing is included, the sign of $\sin \delta$ is positive for $N_c : 0.98(0.94) < N_c < 2.01(1.95)$. Indeed, at the $\pi^+ \pi^-$ invariant mass where the asymmetry, a , is maximum, $\sin \delta = +1$, independent of the parameters used. Thus, by measuring a , we can erase the phase uncertainty $\text{mod}(\pi)$ in the determination of the CKM angle α which arises from the conventional determination of $\sin 2\alpha$.

The theoretical results for the branching ratios for $B^+ \rightarrow \rho^0 \pi^+$ and $B^0 \rightarrow \rho^+ \pi^-$, were compared with the experimental data from the CLEO collaboration [6]. These calculations show that it is possible to have theoretical results consistent with the experimental data without needing to invoke contributions from other resonances [24, 25]. These data helped us to constrain the magnitude of the various form factors needed in the theoretical calcu-

lations of B decays⁴. We determined a range of value of N_c , $0.98(0.94) < N_c < 2.01(1.95)$, inside of which the experimental data and the theoretical calculations are consistent for models 2 and 4.

We will need more accurate data in the future to further decrease the uncertainties in the calculation. If we can use both the CP violating asymmetry and the branching ratios, with smaller uncertainties, we expect to be able to determine the CKM matrix elements more precisely. At the very least, it appears that one will be able to unambiguously determine the sign of $\sin \alpha$ and hence, remove the well known discrete uncertainties in α associated with the fact that indirect CP violation determines only $\sin 2\alpha$. We expect that our predictions should provide useful guidance for future investigations and urge our experimental colleagues to plan seriously to measure the rather dramatic direct CP violation predicted here.

Acknowledgments:

This work was supported in part by the Australian Research Council and the University of Adelaide.

⁴We note that BABAR reported preliminary branching ratios for this channel after this paper was prepared [26]. These results are consistent with the CLEO values.

References

- [1] A.B Carter and A.I. Sanda, Phys. Rev. Lett. **45** (1980) 952, Phys. Rev. **D23** (1981) 1567; I.I. Bigi and A.I. Sanda, Nucl. Phys. **B193** (1981) 85.
- [2] Proceedings of the Workshop on CP Violation, Adelaide 1998, edited by X.-H. Guo, M. Sevier and A.W. Thomas (World Scientific, Singapore).
- [3] R. Enomoto and M. Tanabashi, Phys. Lett. **B386** (1996) 413.
- [4] S. Gardner, H.B. O'Connell and A.W. Thomas, Phys. Rev. Lett. **80** (1998) 1834.
- [5] X.-H. Guo and A.W. Thomas, Phys. Rev. **D58** (1998) 096013, Phys. Rev. **D61** (2000) 116009.
- [6] CLEO Collaboration, hep-ex/0006008.
- [7] G. Buchalla, A.J. Buras and M.E. Lautenbacher, Rev. Mod. Phys. **68**, (1996) 1125.
- [8] N.G. Deshpande and X.-G. He, Phys. Rev. Lett. **74** (1995) 26.
- [9] R. Fleischer, Int. J. Mod. Phys. **A12** (1997) 2459; Z. Phys. **C62** (1994) 81; Z. Phys. **C58** (1993) 483.
- [10] G. Kramer, W. Palmer and H. Simma, Nucl. Phys. **B428** (1994) 77.
- [11] The Particle Data Group, D.E. Groom *et al.*, Eur. Phys. J. **C15** (2000) 1.
- [12] H. B. O'Connell, A.W. Thomas and A.G. Williams, Nucl. Phys. **A623** (1997) 559; K. Maltman, H.B. O'Connell and A.G. Williams, Phys. Lett. **B376** (1996) 19.
- [13] S. Gardner and H.B. O'Connell Phys. Rev. **D57** (1998) 2716.

- [14] L. Wolfenstein, Phys. Rev. Lett. **51** (1983) 1945, Phys. Rev. Lett. **13** (1984) 562.
- [15] M. Bauer, B. Stech and M. Wirbel, Z. Phys. **C34** (1987) 103; M. Wirbel, B. Stech and M. Bauer, Z. Phys. **C29** (1985) 637.
- [16] S. Mele, Phys. Rev. **D59** (1999) 113011.
- [17] F. Parodi, P. Roudeau, and A. Stocchi, Nuovo Cim. **A112** (1999) 833; F. Parodi, invited talk presented at the XXIX International Conference on High Energy Physics, Vancouver, July 23-28.1998; A. Stocchi, hep-ex/9902004.
- [18] X.-H. Guo and T. Huang, Phys. Rev. **D43** (1991) 2931.
- [19] Y.-H. Chen, H.-Y. Cheng, B. Tseng, K.-C. Yang, Phys. Rev. **D60** (1999) 094014.
- [20] P. Ball, hep-ph/9802394.
- [21] P. Ball, V.M. Braun, Phys. Rev. **D58** (1998) 094016.
- [22] M.J. Dugan and B. Grinstein, Phys. Lett. **B255** (1991) 583.
- [23] H.-Y. Cheng, Phys. Lett. **B335** (1994) 428, Phys. Lett. **B395** (1997) 345; H.-Y. Cheng, Phys. Rev. **D58** (1998) 094005.
- [24] A. Deandrea, R. Gatto, M. Ladisa, G. Nardulli and P. Santorelli, hep-ph/0002038.
- [25] A. Deandrea, hep-ph/0005014.
- [26] BABAR Collaboration, hep-ex/0008058.

Figure Captions

Fig.1 Asymmetry, a , for $k^2/m_b^2 = 0.3$, $N_c = 0.98(2.01)$ and limiting values of the CKM matrix elements for model 1: solid line(dot line) for $N_c = 0.98$ and max(min) CKM matrix elements. Dashed line(dot dashed line) for $N_c = 2.01$ and max(min) CKM matrix elements.

Fig.2 Asymmetry, a , for $k^2/m_b^2 = 0.5$, $N_c = 0.94(1.95)$ and limiting values of the CKM matrix elements for model 1: solid line(dot line) for $N_c = 0.94$ and max(min) CKM matrix elements. Dashed line(dot dashed line) for $N_c = 1.95$ and max(min) CKM matrix elements.

Fig.3 Determination of the strong phase difference, $\sin \delta$, for $k^2/m_B^2 = 0.3(0.5)$ and for model 1. Solid line(dot line) for $\tilde{\Pi}_{\rho\omega} = (-3500; -300)$ (i.e. with $\rho - \omega$ mixing). Dot dashed line(dot dot dashed line) for $\tilde{\Pi}_{\rho\omega} = (0; 0)$, (i.e. with no $\rho - \omega$ mixing).

Fig.4 Evolution of the ratio of penguin to tree amplitudes, r , for $k^2/m_B^2 = 0.3(0.5)$, for limiting values of the CKM matrix elements (ρ, η) max(min), for $\tilde{\Pi}_{\rho\omega} = (-3500; -300)(0, 0)$, (i.e. with(without) $\rho - \omega$ mixing) and for model 1. Figure 4a (left): for $\tilde{\Pi}_{\rho\omega} = (0; 0)$, solid line(dot line) for $k^2/m_B^2 = 0.3$ and (ρ, η) max(min). Dot dashed line(dot dot dashed line) for $k^2/m_B^2 = 0.5$ and (ρ, η) max(min). Figure 4b (right): same caption but for $\tilde{\Pi}_{\rho\omega} = (-3500; -300)$.

Fig.5 Branching ratio for $B^0 \rightarrow \rho^+\pi^-$ for models 1(2), $k^2/m_B^2 = 0.3$ and limiting values of the CKM matrix elements. Solid line(dot line) for model 1 and max(min) CKM matrix elements. Dot dashed line(dot dot dashed line) for model 2 and max(min) CKM matrix elements.

Fig.6 Branching ratio for $B^+ \rightarrow \rho^0\pi^+$ for models 1(2), $k^2/m_B^2 = 0.3$ and limiting values of the CKM matrix elements. Solid line(dot line) for model 1 and max(min) CKM matrix elements. Dot dashed line(dot dot dashed line) for model 2 and max(min) CKM matrix elements.

Fig.7 Calculation of the ratio of the two $\rho\pi$ branching ratios versus N_c for models 1(2) and for limiting values of the CKM matrix elements: solid line(dot line) for model 1 with max(min) CKM matrix elements. Dot dashed line(dot dot dashed line) for model 2 with max(min) CKM matrix elements.

Tables

Table 1 Maximum CP violating asymmetry, $a_{max}(\%)$, for $B^+ \rightarrow \pi^+\pi^-\pi^+$, for all models, limiting values of the CKM matrix elements (upper and lower limit), and for $k^2/m_b^2 = 0.3(0.5)$.

Table 2 Values of the CKM unitarity triangle for limiting values of the CKM matrix elements.

Table 3 Summary of the range of values of N_c which is determined from the experimental data for various models and input parameters.

Table 4 Determination of the intersection of the values of N_c which are consistent with various subsets of the data for all models and all sets of CKM matrix elements.

Table 5 Best range of N_c determined from Table 4 for $k^2/m_b^2 = 0.3(0.5)$.

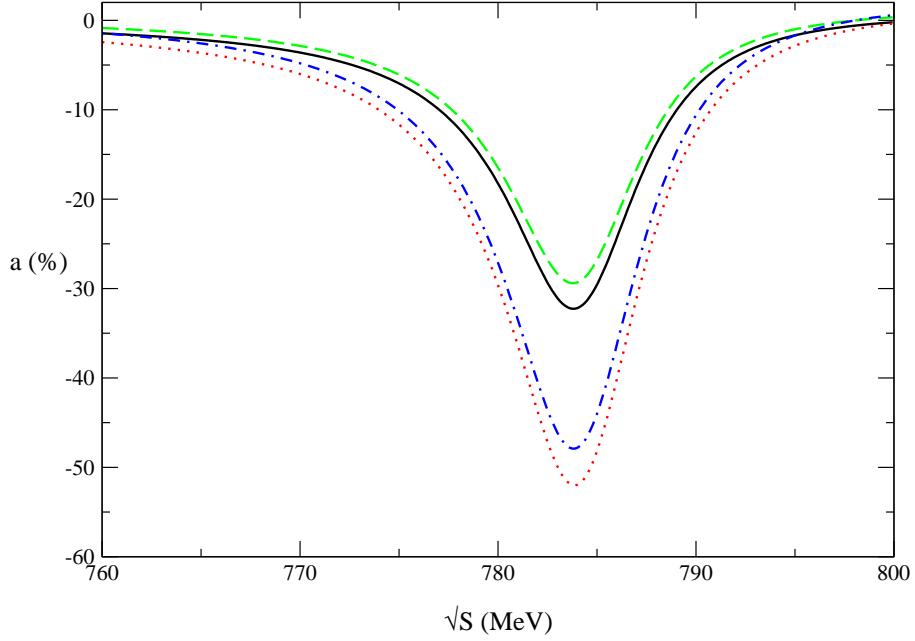


Figure 1: Asymmetry, a , for $k^2/m_b^2 = 0.3$, $N_c = 0.98(2.01)$ and limiting values of the CKM matrix elements for model 1: solid line(dot line) for $N_c = 0.98$ and max(min) CKM matrix elements. Dashed line(dot dashed line) for $N_c = 2.01$ and max(min) CKM matrix elements.

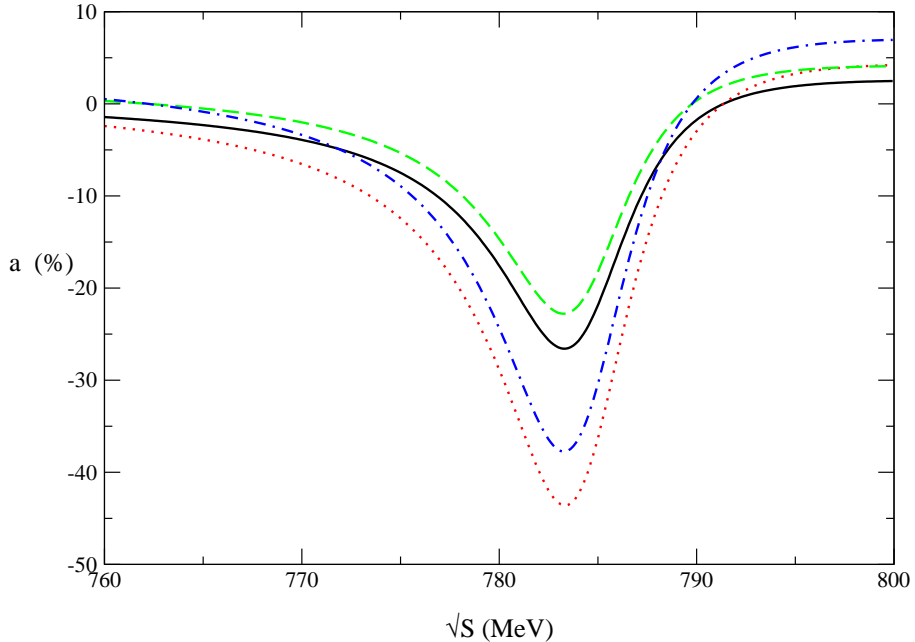


Figure 2: Asymmetry, a , for $k^2/m_b^2 = 0.5$, $N_c = 0.94(1.95)$ and limiting values of the CKM matrix elements for model 1: solid line(dot line) for $N_c = 0.94$ and max(min) CKM matrix elements. Dashed line(dot dashed line) for $N_c = 1.95$ and max(min) CKM matrix elements.

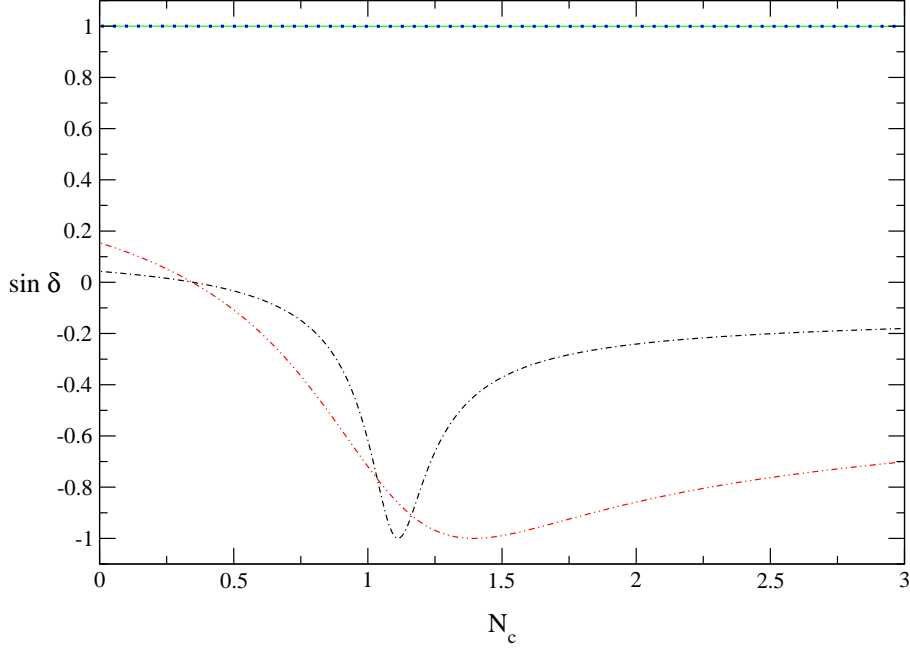


Figure 3: Determination of the strong phase difference, $\sin \delta$, for $k^2/m_B^2 = 0.3(0.5)$ and for model 1. The solid(dotted) line at $\sin \delta = +1$ corresponds the case $\tilde{\Pi}_{\rho\omega} = (-3500; -300)$, where $\rho - \omega$ mixing is included. The dot dashed(dot dot dashed) line corresponds to $\tilde{\Pi}_{\rho\omega} = (0; 0)$, where $\rho - \omega$ mixing is not included.

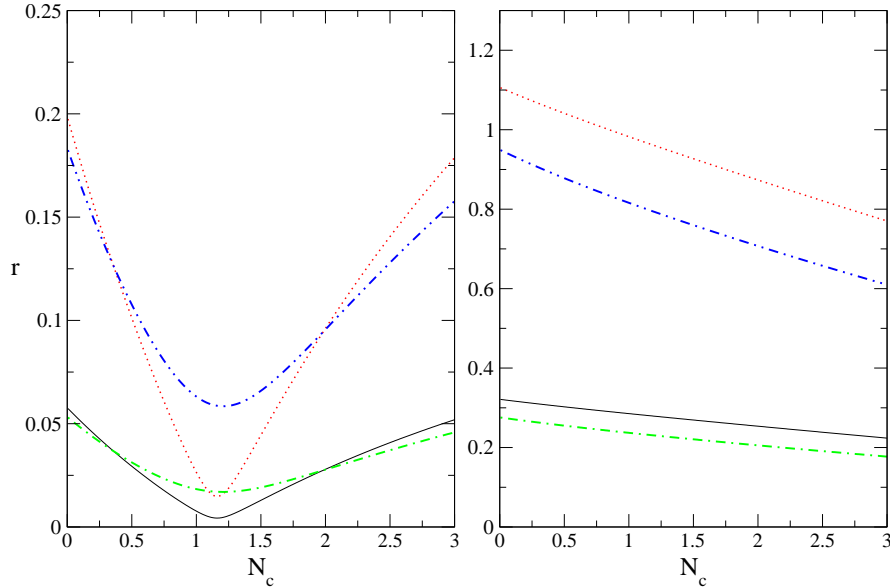


Figure 4: Evolution of the ratio of penguin to tree amplitudes, r , for $k^2/m_B^2 = 0.3(0.5)$, for limiting values of the CKM matrix elements (ρ, η) max(min), for $\tilde{\Pi}_{\rho\omega} = (-3500; -300)(0, 0)$, (i.e. with(without) $\rho - \omega$ mixing) and for model 1. Figure 4a (left): for $\tilde{\Pi}_{\rho\omega} = (0; 0)$, solid line(dot line) for $k^2/m_B^2 = 0.3$ and (ρ, η) max(min). Dot dashed line(dot dot dashed line) for $k^2/m_B^2 = 0.5$ and (ρ, η) max(min). Figure 4b (right): same caption but for $\tilde{\Pi}_{\rho\omega} = (-3500; -300)$.

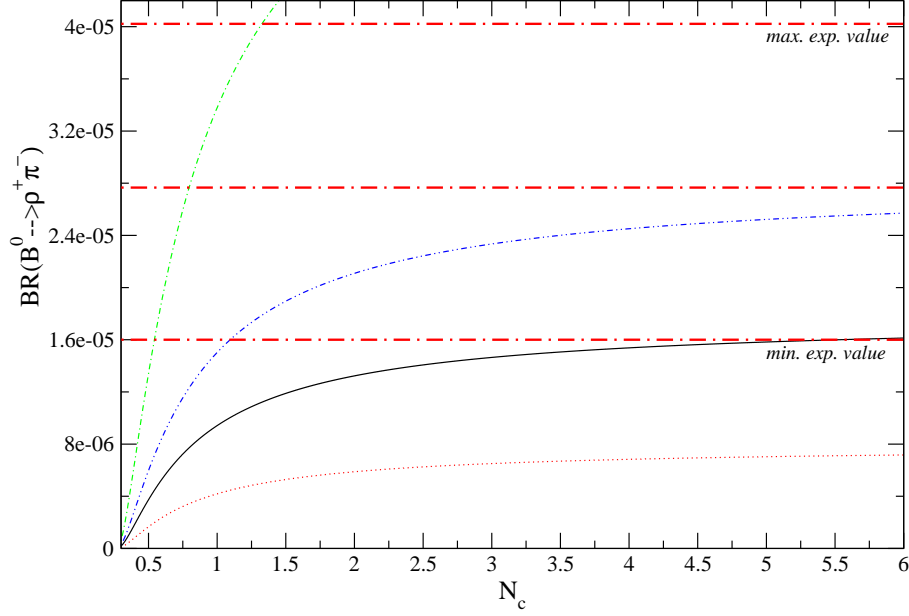


Figure 5: Branching ratio for $B^0 \rightarrow \rho^+ \pi^-$ for models 1(2), $k^2/m_B^2 = 0.3$ and limiting values of the CKM matrix elements. Solid line(dot line) for model 1 and max(min) CKM matrix elements. Dot dashed line(dot dot dashed line) for model 2 and max(min) CKM matrix elements.

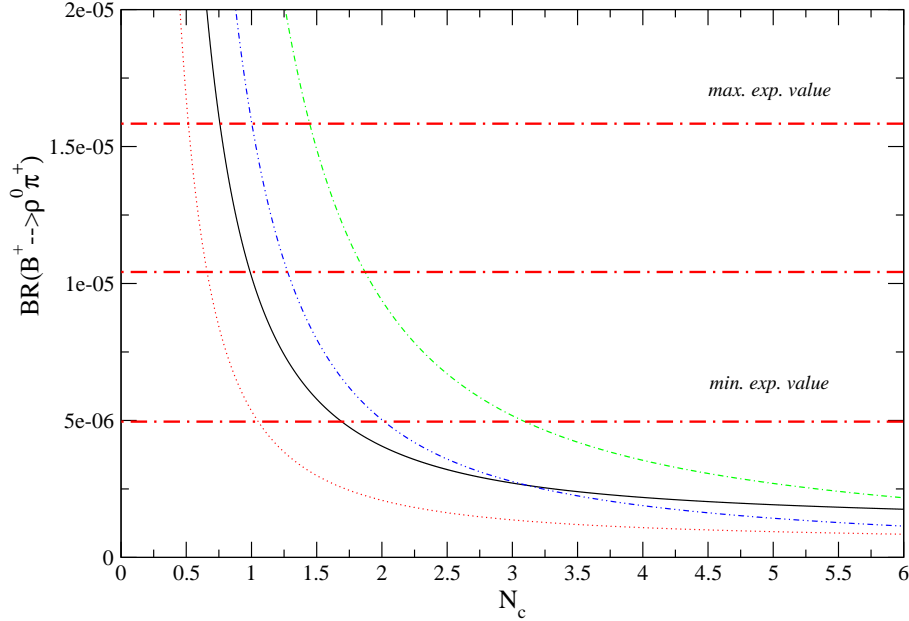


Figure 6: Branching ratio for $B^+ \rightarrow \rho^0 \pi^+$ for models 1(2), $k^2/m_B^2 = 0.3$ and limiting values of the CKM matrix elements. Solid line(dot line) for model 1 and max(min) CKM matrix elements. Dot dashed line(dot dot dashed line) for model 2 and max(min) CKM matrix elements.

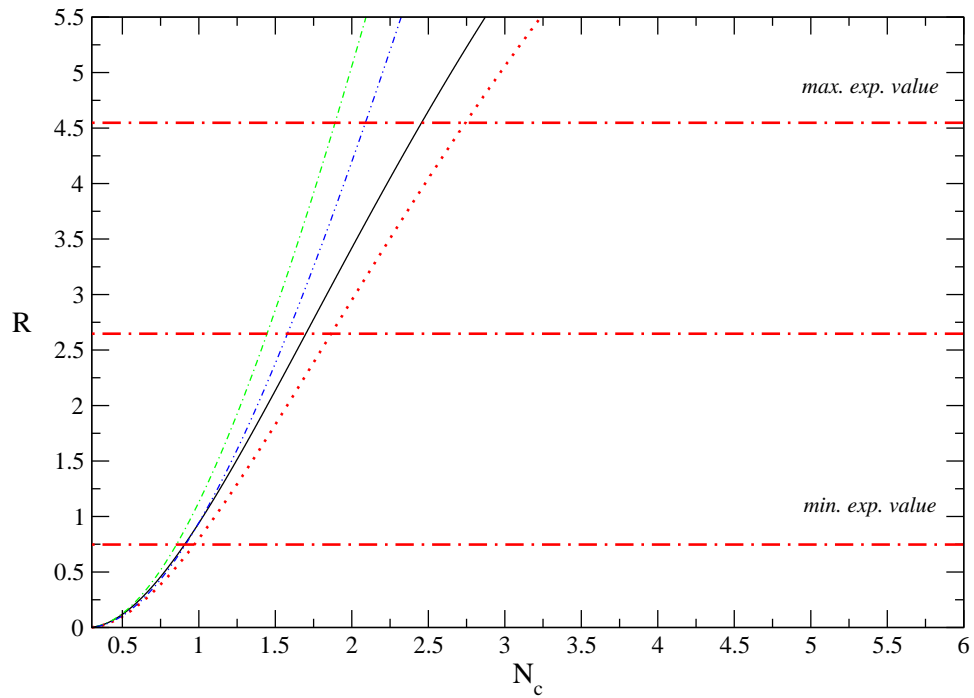


Figure 7: Calculation of the ratio of two $\rho\pi$ branching ratios versus N_c for models 1(2) and for limiting values of the CKM matrix elements: solid line(dot line) for model 1 with max(min) CKM matrix elements. Dot dashed line(dot dot dashed line) for model 2 with max(min) CKM matrix elements.

$N_{cmin} = 0.98(0.94) \quad N_{cmax} = 2.01(1.95)$		
model 1		
ρ_{max}, η_{max}	-33(-27)	-29(-23)
ρ_{min}, η_{min}	-52(-43)	-47(-37)
model 2		
ρ_{max}, η_{max}	-36(-29)	-37(-28)
ρ_{min}, η_{min}	-57(-48)	-59(-46)
model 3		
ρ_{max}, η_{max}	-32(-26)	-29(-23)
ρ_{min}, η_{min}	-51(-43)	-47(-37)
model 4		
ρ_{max}, η_{max}	-36(-29)	-37(-28)
ρ_{min}, η_{min}	-57(-48)	-59(-46)
model 5		
ρ_{max}, η_{max}	-29(-24)	-24(-19)
ρ_{min}, η_{min}	-48(-40)	-39(-31)

Table 1: Maximum CP violating asymmetry $a_{max}(\%)$ for $B^+ \rightarrow \pi^+\pi^-\pi^+$, for all models, limiting values of the CKM matrix elements (upper and lower limit), and for $k^2/m_b^2 = 0.3(0.5)$.

	$(\rho, \eta)_{min}$	$(\rho, \eta)_{max}$
α	86°02	89°23
β	19°50	30°64
γ	74°43	60°11

Table 2: Values of the CKM unitarity triangle for limiting values of the CKM matrix elements.

	B^+	B^0	R
model 1			
ρ_{max}, η_{max}	0.76;1.69(0.73;1.62)	5.50; ** (- ; -)	0.92;2.57(0.90;2.52)
ρ_{min}, η_{min}	0.52;1.04(0.49;0.98)	- ; - (- ; -)	0.97;2.88(0.94;2.76)
ρ_{max}, η_{min}	0.61;1.25(0.59;1.20)	- ; - (- ; -)	0.92;2.58(0.91;2.54)
ρ_{min}, η_{max}	0.69;1.46(0.66;1.39)	- ; - (- ; -)	0.95;2.75(0.90;2.66)
model 2			
ρ_{max}, η_{max}	1.44;3.06(1.40;2.95)	0.54;1.33(0.54;1.38)	0.86;1.89(0.84;1.86)
ρ_{min}, η_{min}	1.00;2.01(0.96;1.90)	1.10; ** (1.15; **)	0.92;2.09(0.89;2.01)
ρ_{max}, η_{min}	1.15;2.32(1.12;2.22)	0.70; ** (0.72; **)	0.87;1.89(0.85;1.86)
ρ_{min}, η_{max}	1.32;2.78(1.25;2.60)	0.63;2.77(0.62;3.12)	0.90;2.00(0.84;1.94)
model 3			
ρ_{max}, η_{max}	0.74;1.65(0.72;1.60)	- ; - (- ; -)	0.92;2.65(0.92;2.60)
ρ_{min}, η_{min}	0.51;1.02(0.49;0.98)	- ; - (- ; -)	0.97;2.95(0.94;2.85)
ρ_{max}, η_{min}	0.60;1.22(0.57;1.19)	- ; - (- ; -)	0.93;2.66(0.92;2.61)
ρ_{min}, η_{max}	0.67;1.43(0.65;1.37)	- ; - (- ; -)	0.92;2.79(0.92;2.71)
model 4			
ρ_{max}, η_{max}	1.41;3.04(1.36;2.92)	0.56;1.44(0.57;1.52)	0.86;1.91(0.85;1.87)
ρ_{min}, η_{min}	0.98;1.96(0.94;1.87)	1.16; ** (1.23; **)	0.90;2.10(0.89;2.03)
ρ_{max}, η_{min}	1.14;2.29(1.10;2.21)	0.72; ** (0.74; **)	0.86;1.92(0.85;1.88)
ρ_{min}, η_{max}	1.30;2.74(1.24;2.59)	0.64;3.49(0.66;4.03)	0.89;2.01(0.86;1.95)
model 5			
ρ_{max}, η_{max}	0.75;2.18(0.73;2.10)	- ; - (- ; -)	1.03; ** (1.02; **)
ρ_{min}, η_{min}	0.50;1.08(0.47;1.03)	- ; - (- ; -)	1.09; ** (1.06; **)
ρ_{max}, η_{min}	0.58;1.38(0.55;1.34)	- ; - (- ; -)	1.03; ** (1.02; **)
ρ_{min}, η_{max}	0.66;1.71(0.64;1.62)	- ; - (- ; -)	1.04; ** (1.04; **)

Table 3: Summary of the range of values of N_c which is determined from the experimental data for various models and input parameters (numbers outside(inside) brackets are for $k^2/m_b^2 = 0.3(0.5)$). The notation: (number ; number) means that there is a upper and lower limit for N_c . (number ; **) means that there is no upper limit for N_c in the range $N_c [0;10]$. (- ; -) means that there is no range of N_c which is consistent with experimental data.

	$\{N_c\}_{B^+} \cap \{N_c\}_{B^0}$	$\{N_c\}_{B^+} \cap \{N_c\}_R$	$\{N_c\}_{B^0} \cap \{N_c\}_R$
model 1			
ρ_{max}, η_{max}	– (–)	0.92;1.69(0.90;1.62)	– (–)
ρ_{min}, η_{min}	– (–)	0.97;1.04(0.94;0.98)	– (–)
ρ_{max}, η_{min}	– (–)	0.92;1.25(0.91;1.20)	– (–)
ρ_{min}, η_{max}	– (–)	0.95;1.46(0.90;1.39)	– (–)
model 2			
ρ_{max}, η_{max}	– (–)	1.44;1.89(1.40;1.86)	0.86;1.33(0.84;1.38)
ρ_{min}, η_{min}	1.10;2.01(1.15;1.90)	1.00;2.01(0.96;1.90)	1.10;2.09(1.15;2.01)
ρ_{max}, η_{min}	1.15;2.32(1.12;2.22)	1.15;1.89(1.12;1.86)	0.87;1.89(0.85;1.86)
ρ_{min}, η_{max}	1.32;2.78(1.25;2.60)	1.32;2.00(1.25;1.94)	0.90;2.00(0.84;1.94)
model 3			
ρ_{max}, η_{max}	– (–)	0.92;1.65(0.92;1.60)	– (–)
ρ_{min}, η_{min}	– (–)	0.97;1.02(0.94;0.98)	– (–)
ρ_{max}, η_{min}	– (–)	0.93;1.22(0.92;1.19)	– (–)
ρ_{min}, η_{max}	– (–)	0.92;1.43(0.92;1.37)	– (–)
model 4			
ρ_{max}, η_{max}	1.41;1.44(1.36;1.52)	1.41;1.91(1.36;1.87)	0.86;1.44(0.85;1.52)
ρ_{min}, η_{min}	1.16;1.96(1.23;1.87)	0.98;1.96(0.94;1.87)	1.16;2.10(1.23;2.03)
ρ_{max}, η_{min}	1.14;2.29(1.10;2.21)	1.14;1.92(1.10;1.88)	0.86;1.92(0.85;1.88)
ρ_{min}, η_{max}	1.30;2.74(1.24;2.59)	1.30;2.01(1.24;1.95)	0.89;2.01(0.86;1.95)
model 5			
ρ_{max}, η_{max}	– (–)	1.03;2.18(1.02;2.10)	– (–)
ρ_{min}, η_{min}	– (–)	– (–)	– (–)
ρ_{max}, η_{min}	– (–)	1.03;1.38(1.02;1.34)	– (–)
ρ_{min}, η_{max}	– (–)	1.04;1.71(1.04;1.62)	– (–)

Table 4: Determination of the intersection of the values of N_c which are consistent with various subsets of the data for all models and all sets of CKM matrix elements (numbers outside(inside) brackets are for $k^2/m_b^2 = 0.3(0.5)$). The notation:

– (–) means that no common range of N_c can be extracted from the data.

	$\{N_c\}$ with mixing	$\{N_c\}$ without mixing
model 2	1.00;2.01(0.96;1.94)	0.85;1.74(0.85;1.74)
model 4	0.98;2.01(0.94;1.95)	0.84;1.76(0.84;1.75)
maximum range	0.98;2.01(0.94;1.95)	0.84;1.76(0.84;1.75)
minimum range	1.00;2.01(0.96;1.94)	0.85;1.74(0.85;1.74)

Table 5: Best range of N_c determined from Table 4 for $k^2/m_b^2 = 0.3(0.5)$. One takes the maximum interval of N_c , from Table 4, for each model (2,4). To determine the maximum(minimum) range, one considers all models (2,4) and the largest(smallest) range of N_c . In comparison, we show the range of N_c determined without $\rho - \omega$ mixing.